

Strong correlation between structure and magnetic ordering in tetragonally distorted off-stoichiometric spinels $\text{Mn}_{1.15}\text{Co}_{1.85}\text{O}_4$ and $\text{Mn}_{1.17}\text{Co}_{1.60}\text{Cu}_{0.23}\text{O}_4$

P. Pramanik¹, M. Reehuis², M. Tovar², A. Hoser², J.-U. Hoffmann², Y. S. Chen³, J. G. Lin³, B. Weise⁴, A. Waske⁴, and S. Thota^{1,*}

¹Department of Physics, Indian Institute of Technology Guwahati-781039, Assam, India

²Helmholtz-Zentrum Berlin für Materialien und Energie, Hahn-Meitner-Platz 1, D-14109 Berlin, Germany

³Center for Condensed Matter Sciences, National Taiwan University, Taipei 10617, Taiwan

⁴Leibniz-IFW Dresden, Institute for Complex Materials, D-01069 Dresden, Germany

 (Received 3 June 2021; revised 7 December 2021; accepted 4 March 2022; published 28 March 2022)

We report a systematic study on the structural and magnetic properties of off-stoichiometric polycrystalline bulk spinels $\text{Mn}_{1.15}\text{Co}_{1.85}\text{O}_4$ and $\text{Mn}_{1.17}\text{Co}_{1.60}\text{Cu}_{0.23}\text{O}_4$ using neutron and x-ray diffraction, ferromagnetic resonance, and magnetic measurements. Both compounds show a weak tetragonal distortion with $c/a < 1$, where the crystal structure could be refined in the tetragonal space group $I4_1/amd$. Both Co^{2+} and Cu^{2+} ions are located at the tetrahedral A site, and Mn^{3+} and Co^{3+} at the octahedral B site. Ferrimagnetic (FI) ordering of $\text{Mn}_{1.15}\text{Co}_{1.85}\text{O}_4$ and $\text{Mn}_{1.17}\text{Co}_{1.60}\text{Cu}_{0.23}\text{O}_4$ sets in below 184 and 164 K, respectively. Magnetic structure analysis revealed that the ferrimagnetically coupled A^{2+} - and B^{3+} -site moments are aligned parallel to the tetragonal c axis. Additionally, a noncollinear antiferromagnetic order appears in the ab plane, where the moments point along $[110]$ and $[1\bar{1}0]$. The net magnetic moment $[2\mu_{\text{FI}}(\text{Mn}_B/\text{Co}_B) - \mu_{\text{FI}}(\text{Co}_A)]$ of $\text{Mn}_{1.15}\text{Co}_{1.85}\text{O}_4$ obtained from neutron data varies between 0.88–1.08 μ_B which is in good agreement with $M = 0.89$ –1.13 μ_B as determined from magnetization measurements. However, for the Cu-containing compound a larger discrepancy in the magnetic moment was observed between the neutron data (1.89–1.92 μ_B) and low-temperature ($T = 1.9$ K) field-dependent ($H = 90$ kOe) magnetization data (0.97–1.21 μ_B). From the three-sublattice model we obtained canting angles 28° and 25° for $\text{Mn}_{1.15}\text{Co}_{1.85}\text{O}_4$ and $\text{Mn}_{1.17}\text{Co}_{1.60}\text{Cu}_{0.23}\text{O}_4$, respectively. Both the bulk systems exhibit high magnetocrystalline anisotropy ($K_U \sim 9 \times 10^5$ and 7.5×10^5 erg/cm³) and a field-induced transition (H_D) across 4.0 kOe due to the domain reorientation. Temperature (1.9–350 K) and field (± 90 kOe) dependence of magnetization data confirms the high-spin ($S = \frac{3}{2}$ and $S = 2$) ground-state configuration for both the divalent Co and trivalent Mn.

DOI: [10.1103/PhysRevMaterials.6.034407](https://doi.org/10.1103/PhysRevMaterials.6.034407)

I. INTRODUCTION

Ferrimagnetic spinel oxides belong to a well-known class which shows intriguing low-temperature magnetic behavior such as geometrical frustration, Jahn-Teller distortion, magnetoelectric coupling, tunable exchange bias, reentrant spin glass, and negative magnetization including compensation phenomena [1–14]. Such complex magnetic ordering frequently noticed in Mn-, Co-, and Cr-based spinel systems like $\text{Co}_{3-x}\text{Mn}_x\text{O}_4$, ZnMn_2O_4 , $\text{Mn}_{3-x}\text{Cu}_x\text{O}_4$, and CoCr_2O_4 and variety of other systems which crystallizes in pyrochlore lattice [5,8,15–17]. On the other hand, these compounds in the form of low-dimensional nanostructures have drawn immense attention recently because of their wide applications in the renewable energy sector [18–21]. In particular, the inverse spinel MnCo_2O_4 has received widespread attention because of its diverse applications and novel magnetic properties [22–27]. The ferrimagnetic behavior (still dominant A - B interaction) in this compound arises due to the unequal moments of trivalent Mn and Co as well as divalent Co described by a formula unit $(\text{Co}^{2+})_A[\text{Co}^{3+}\text{Mn}^{3+}]_B\text{O}_4$ [28].

Previous studies by Wickham and Croft reported long-range ordering in this compound with ordering temperatures as high as 191 K for $\text{Mn}_{1.2}\text{Co}_{1.8}\text{O}_4$, but Blasse *et al.* reported slightly lesser ordering temperatures ~ 170 K for stoichiometric MnCo_2O_4 [28,29]. Recent studies reported enhanced multiferroic properties in the Bi- and Y-substituted MnCo_2O_4 [$\text{Bi}_x\text{Co}_{2-x}\text{MnO}_4$ ($0 \leq x \leq 0.3$) and $\text{Y}_x\text{Co}_{2-x}\text{MnO}_4$ ($0 \leq x \leq 0.2$)] in great detail [30,31]. Han *et al.* reported ferroelectricity at room temperature and enhanced ferrimagnetic ordering temperature ($T_C \sim 186$ K) in Y-substituted MnCo_2O_4 spinel [31]. Conversely, a significant decrease of T_C (167 and 165 K) and average magnetic moment (7.51 and 7.9 μ_B) has been observed in Cu- and Zn-substituted MnCo_2O_4 [32,33]. Moreover, these compounds under nanostructures exhibit spin-glass-like characteristics with further reduction in T_C (155 and 157 K) [32,33].

Initial studies by Joy and Date reported unusual hysteresis behavior in bulk MnCo_2O_4 system in which the anisotropy field overcomes the coercivity below 130 K due to the irreversible domain wall movements due to the rearrangement of the valence electrons [26]. Such uncommon magnetic character of this system combined with the off-stoichiometry ($\text{MnCo}_2\text{O}_{4+\delta}$) arising at the stage of preparation leads to significant alteration in the magnetic exchange interactions and

*subhasht@iitg.ac.in

the long-range ordering temperature of the system [26,34]. Also, pressure ($P \leq 1.71$ GPa) driven changes such as Hopkinson effect in terms of the cusp in temperature dependence of relative magnetic permeability $\mu_r(T)$ across 175 K and influence of finite-size and surface effects on the magnetic properties are the unique characteristic features of the current system [25]. Moreover, the composites based on MnCo_2O_4 system are having a wide range of applications in fuel cells and Li-ion batteries which makes them an active field of research not only from the fundamental point of view, which is one of the motivating factors to reinvestigate this system. Usually, the Jahn-Teller (JT) active unoccupied e_g orbital ions such as divalent Cu^{2+} ($3d^9$) and trivalent Mn^{3+} ($3d^4$) stabilizes the tetragonal symmetry ($c > a\sqrt{2}$) by introducing large octahedral crystal field at the B sites. We anticipate that such tetragonal elongations moderately lift the crystal symmetry, thereby causing geometrical frustrations in the spinel lattice which significantly alters the exchange interactions as the bond distance changes. Hence, the introduction of such JT ions unequivocally hosts the orthorhombic strains in the ground state with doubly degenerate d_{xz}/d_{yz} orbitals causing a drastic change in the magnetic ordering, which is the primary motivation of incorporating Cu in the spinel lattice of MnCo_2O_4 . Also, the determination of the accurate cationic distribution by neutron diffraction and its magnetic characterization is an important aspect which essentially decides the limit to each site occupancy. Nevertheless, a detailed study on this system focusing the local distortions and site-dependent magnetic moments at various temperatures below T_C using the neutron diffraction experiments are rare in the literature. Mandrus *et al.* first reported powder neutron diffraction studies on $\text{Co}_2\text{Ru}_{1-x}\text{Mn}_x\text{O}_4$ system in which they reported two transitions at 100 and 180 K providing the evidence for short-ranged correlations (length of about 100 Å) below the ferrimagnetic ordering [35]. For moderate Ru³⁺ ($S = \frac{1}{2}$) content ($x \geq 0.5$), Granroth *et al.* reported that a ground state is a mixture of long-range ferrimagnetic order with the short-range order, however, for lower Ru content the system exhibits long-range order [36]. For complete Mn dilution with Ru leads to spin-glass-like characteristics with spin-freezing temperatures as low as 16 K [35]. Neutron diffraction study on Bi-doped MnCo_2O_4 by Kaushik *et al.* revealed significant increase in the T_C (200 K), Co-O bond length, and relaxation in the CoO_6 polyhedra [37]. Except in these two papers there is no detailed neutron diffraction study on MnCo_2O_4 -related systems available in the literature. Therefore, in this work we report extensive investigations of the crystal structure and magnetic behavior of $\text{Mn}_{1.15}\text{Co}_{1.85}\text{O}_4$ and $\text{Mn}_{1.17}\text{Co}_{1.60}\text{Cu}_{0.23}\text{O}_4$ polycrystalline spinels using neutron scattering, bulk magnetization measurements, and ferromagnetic resonance (FMR). These studies are primarily aimed at a detailed understanding of the crystal structure, magnetic ordering, and the role of Cu substitution. Moreover, we explore the magnetization processes and thermal evolution of the magnetic moments of the individual A - and B -site atoms.

II. EXPERIMENTAL DETAILS

Polycrystalline spinel oxides of manganese cobalt oxide and a copper-doped sample were prepared by the solid-state

reaction method using the binary transition metal oxides Co_3O_4 , Mn_2O_3 , and CuO as precursors. Appropriate amounts of these precursors were ground in an agate mortar for 6 h and pelletized using a hydraulic press with 50-kN pressure. These cylindrical pellets are finally sintered at 1200 °C for 8 h duration with 4 °C per minute heating and cooling rates. The structural characterization and phase purity of the sintered pellets were carried out by using a Rigaku x-ray diffractometer (model: TRAX III) with $\text{Cu-K}\alpha$ radiation ($\lambda = 1.54056$ Å) at room temperature. For further investigations of the crystal structure at 15 and 295 K we used a Guinier diffractometer Huber 645 ($\text{Cu-K}\alpha_1$, $\lambda = 1.5406$ Å), where x-ray powder data were collected in the 2θ range between 15° and 100°.

Neutron powder diffraction experiments on these samples were carried out on the instruments E2 [38], E6, and E9 [39] at the BER II reactor of the Helmholtz-Zentrum Berlin. The instrument E9 uses a Ge monochromator selecting the neutron wavelength $\lambda = 1.301$ Å, while the instruments E2 and E6 use a pyrolytic graphite (PG) monochromator selecting the neutron wavelengths $\lambda = 2.379$ and 2.423 Å, respectively. On these instruments, powder patterns were recorded between the following diffraction angles: between 14.7° and 90.2° (E2), 5.5° and 136.6° (E6), and 5° and 141.8° (E9). The instrument E9 was used to investigate the crystal structure at 3 and 295 K. In order to investigate in detail the magnetic structure of both compounds, neutron powder diffraction patterns were collected at $T = 1.7$ K on the instrument E2 with high counting statistics (24 h/pattern) using a 15-min collimation to improve the instrumental resolution. In the paramagnetic range, a second powder pattern was collected at 200 K. The temperature-dependent behavior of the magnetic ordering has been investigated on the instrument E6. The refinements of crystal and magnetic structures were carried out with the FULLPROF program [40]. The nuclear scattering lengths $b(\text{O}) = 5.805$ fm, $b(\text{Mn}) = -3.73$ fm, $b(\text{Co}) = 2.50$ fm, and $b(\text{Cu}) = 7.718$ fm were used [41]. The magnetic form factors of the Mn^{3+} , Co^{2+} , and Co^{3+} ions were taken from Ref. [42]. All the magnetization and heat-capacity measurements are performed using physical property measurement system (PPMS) based vibrating sample magnetometer (VSM) from Quantum Design (Dynacool model).

III. RESULTS AND DISCUSSION

A. Crystal structure

In an earlier study it was shown that the inverse spinel TiCo_2O_4 was found to crystallize in the cubic space group $Fd\bar{3}m$ (No.227) [43], while the Mn-containing compounds $\text{Ti}_{0.8}\text{Mn}_{0.2}\text{Co}_2\text{O}_4$ and $\text{Ti}_{0.6}\text{Mn}_{0.4}\text{Co}_2\text{O}_4$ crystallize in the tetragonal space group $I4_1/amd$ (No. 141, cell choice 2) with the cell dimensions $a_t \times b_t \times c_t = a_c/\sqrt{2} \times b_c/\sqrt{2} \times c_c$ [44]. Although Rietveld refinements of the neutron powder data revealed a c/a ratio slightly smaller than 1, a splitting of Bragg reflections could not be clearly observed. From our refinements of the neutron powder data (collected on the instrument E9) we noticed the same trend for present compounds. This led us to investigate the degree of tetragonal splitting in more detail with a Guinier diffractometer which enables a much better instrumental resolution than

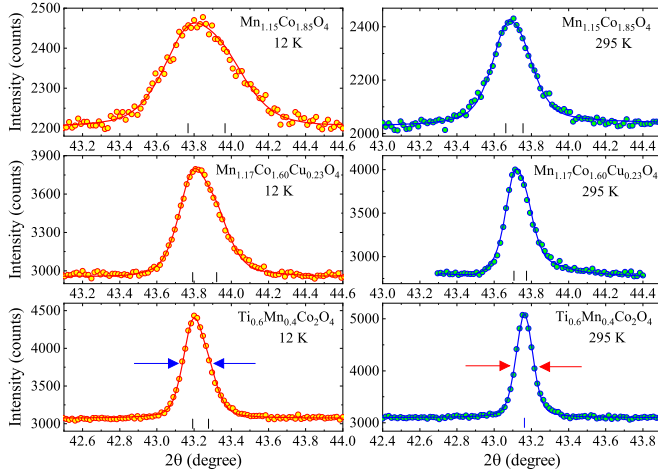


FIG. 1. Tetragonal splitting of $\text{Mn}_{1.15}\text{Co}_{1.85}\text{O}_4$ and $\text{Mn}_{1.17}\text{Co}_{1.60}\text{Cu}_{0.23}\text{O}_4$ determined from Guinier-powder-diffraction data. In both compounds, the cubic reflection (400) splits into the tetragonal ones (220) and (004) which additionally show a superimposed intrinsic peak broadening. Therefore, the peak profiles are compared with those of $\text{Ti}_{0.6}\text{Mn}_{0.4}\text{Co}_2\text{O}_4$, where no tetragonal splitting occurs, and the intrinsic peak broadening is much less pronounced. The calculated patterns (solid lines) are compared with the observed one (circles). In the lower part of each diagram the positions of the reflections (400)/(040) and (004) (black bars) are shown.

the neutron diffractometer E9. For comparison, we have also collected x-ray powder data of $\text{Ti}_{0.6}\text{Mn}_{0.4}\text{Co}_2\text{O}_4$. For this compound the $c_t/a_t\sqrt{2}$ ratios 0.99819(6) and 0.99992(9) have been obtained at 12 and 295 K, respectively. These values could be determined with better accuracy than the ratios $c_t/a_t\sqrt{2} = 0.9988(3)$ and $c_t/a_t\sqrt{2} = 0.9995(3)$ obtained earlier at 3 and 295 K [44]. This clearly indicates that a tetragonal distortion of $\text{Ti}_{0.6}\text{Mn}_{0.4}\text{Co}_2\text{O}_4$ only occurs in the magnetically ordered range, whereas its structure remains cubic at room temperature. The evidence of a tetragonal distortion results in a splitting of the cubic (400) into the tetragonal reflections (220)/(2 $\bar{2}$ 0) and (004) giving an intensity ratio of 2 : 1. Therefore, this reflection changes at 12 K to a broader asymmetric peak caused by the presence of a tetragonal splitting as shown in Fig. 1. Unfortunately, the Bragg reflections of $\text{Mn}_{1.15}\text{Co}_{1.85}\text{O}_4$ and $\text{Mn}_{1.17}\text{Co}_{1.60}\text{Cu}_{0.23}\text{O}_4$ show a superimposed intrinsic broadening, where the broadening is more pronounced in $\text{Mn}_{1.15}\text{Co}_{1.85}\text{O}_4$. This may be ascribed to an inhomogeneity or strain effects in the sample. Thus, an asymmetric peak shape is difficult to observe for $\text{Mn}_{1.15}\text{Co}_{1.85}\text{O}_4$ at 295 K. Nevertheless, a tetragonal splitting could be found for both compounds from the Rietveld refinements of the data sets collected at 12 and 295 K. This indicates that the tetragonal distortion may be ascribed to ionic-size effects. The lattice parameters are shown in Table I. On the other hand, it can be seen in Fig. 1 that the peak broadening

TABLE I. Results of the Rietveld refinements of the x-ray and neutron powder diffraction data of $\text{Mn}_{1.15}\text{Co}_{1.85}\text{O}_4$ and $\text{Mn}_{1.17}\text{Co}_{1.60}\text{Cu}_{0.23}\text{O}_4$ collected on the instrument E9 at 3 and 295 K. The refinements were carried out in the tetragonal space group $I4_1/amd$. The given residuals are defined as $R_F = \frac{\sum |F_{\text{obs}}| - |F_{\text{calc}}|}{\sum |F_{\text{obs}}|}$. Listed are the positional parameters y and z of the O atom located at the site $16h(0,y,z)$ and the occupancies of the Mn_B and Co_B atoms at the site $8c(0,0,0)$. Further, the bond distances in the $T_B\text{O}_6$ octahedra ($T_B = \text{Mn}_B$ and Co_B), and the $T_A\text{O}_4$ tetrahedra ($T_A\text{O}_4 = \text{Co}_A$ and Cu_A) as well as the lattice parameters are also given.

	$\text{Mn}_{1.15}\text{Co}_{1.85}\text{O}_4$		$\text{Mn}_{1.17}\text{Co}_{1.60}\text{Cu}_{0.23}\text{O}_4$	
T (K)	3/15 ^a	295	3/15 ^a	295
$occ(\text{Mn}_B)$	1.125(6)	1.145(7)	1.180(9)	1.173(7)
$occ(\text{Co}_B)$	0.875(6)	0.852(7)	0.820(9)	0.829(6)
$y(\text{O})$	0.5273(4)	0.5243(5)	0.5257(7)	0.5236(9)
$z(\text{O})$	0.2409(5)	0.2382(5)	0.2417(8)	0.2388(9)
a_t (Å)	5.8526(6)	5.8643(4)	5.8443(5)	5.8522(6)
c_t (Å)	8.2582(14)	8.2721(12)	8.2374(16)	8.2562(16)
$c_t/a_t\sqrt{2}$	0.9977(3)	0.9974(2)	0.9966(3)	0.9976(3)
V (Å ³)	282.87(7)	284.47(6)	281.36(7)	282.76(8)
a_t (Å) ^a	5.8550(3)	5.8626(3)	5.8433(2)	5.8532(2)
c_t (Å) ^a	8.2514(6)	8.2759(6)	8.2411(3)	8.2553(3)
$c_t/a_t\sqrt{2}$ ^a	0.99653(13)	0.99818(12)	0.99726(6)	0.99730(6)
V (Å ³) ^a	282.86(4)	284.45(3)	281.38(2)	282.83(2)
$d_{\text{eq}}(T_B\text{-O}) \times 4$	1.961(2)	1.977(2)	1.964(3)	1.976(4)
$d_{\text{ap}}(T_B\text{-O}) \times 2$	1.997(4)	1.976(4)	1.996(7)	1.976(8)
$\angle_{\text{eq}}(\text{O}-T_B-\text{O})(^\circ) \times 4$	84.4(2)	84.1(2)	84.8(4)	84.4(5)
$\angle_{\text{ap}}(\text{O}-T_B-\text{O})(^\circ) \times 2$	83.32(7)	83.03(9)	83.73(13)	84.24(18)
$d(\text{Co}_A\text{-O}) \times 4$	1.964(3)	1.967(3)	1.950(5)	1.957(7)
$\angle_{ab}(\text{O}-\text{Co}_A\text{-O})(^\circ) \times 4$ [§]	108.5(2)	109.7(2)	108.5(5)	109.3(5)
$\angle_c(\text{O}-\text{Co}_A\text{-O})(^\circ) \times 2$ [§]	111.42(10)	109.75(10)	111.45(15)	109.82(20)
R_F	0.042	0.036	0.043	0.043

^aFrom x-ray data; [§] for $\angle_{ab}(\text{O}-\text{Co}_A\text{-O})$ the angle bisector is lying within the ab plane, and for $\angle_c(\text{O}-\text{Co}_A\text{-O})$ it points along c .

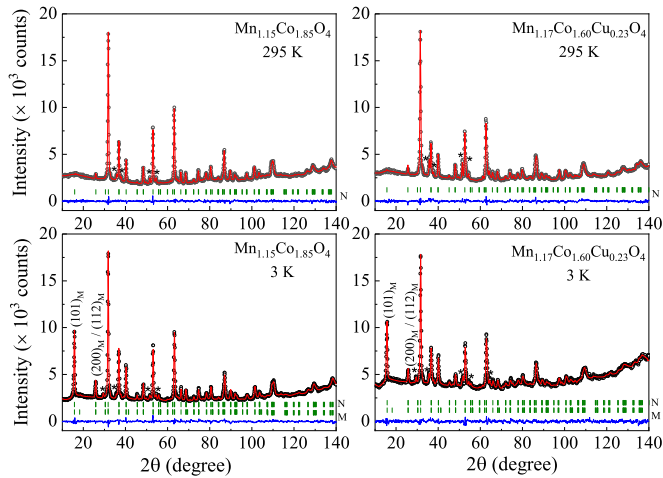


FIG. 2. Rietveld refinements of the neutron powder diffraction data of $\text{Mn}_{1.15}\text{Co}_{1.85}\text{O}_4$ and $\text{Mn}_{1.17}\text{Co}_{1.60}\text{Cu}_{0.23}\text{O}_4$ collected on E9 at 295 and 3 K, respectively. The crystal structure was refined in the tetragonal space group $I4_1/amd$. The calculated patterns (red line) are compared with the observed one (black open circles). In the lower part of each diagram, the difference pattern (blue line) as well as the positions of the nuclear (N) and magnetic (M) reflections of are shown. A strongest magnetic contribution is observed for the reflections (101) and (200)/(112). Both samples contain some impurities of CoO and Co_3O_4 . The strongest reflections (nuclear and magnetic) are marked with an asterisk.

of both compounds is more pronounced at 12 K. Here, it is interesting to see that the presence of ferrimagnetic ordering leads to an increased peak broadening again. This may be ascribed to superimposed magnetoelastic effects.

Figure 2 shows the neutron powder diffraction patterns of the two samples $\text{Mn}_{1.15}\text{Co}_{1.85}\text{O}_4$ and $\text{Mn}_{1.17}\text{Co}_{1.60}\text{Cu}_{0.23}\text{O}_4$ collected on the instrument E9 at 3 and 295 K. In the patterns collected at 3 K, additional magnetic intensities are observed, where the strongest magnetic contribution is observed at the positions of the reflections (101) and (200)/(112) (see also Fig. 4). Both samples contain small amounts of the impurities Co_3O_4 and CoO which were additionally formed during the preparation stage. For the Rietveld refinements, we have taken into account the structural and magnetic parameters of these compounds given in Refs. [45,46]. Refinements have also been performed in the lower symmetric space group $I4_1/amd$. In this structure the Co^{2+} ions occupy the tetrahedral A site, while Mn^{3+} and Co^{3+} ions are statistically distributed on the octahedral B site. For the copper-containing sample the Cu^{2+} ions are also expected to be located at the A site since the ionic radii of Co^{2+} ($r = 0.58 \text{ \AA}$) and Cu^{2+} ($r = 0.57 \text{ \AA}$) are practically the same [47]. In fact, the refinement of the occupancy of the A site resulted in a too large value if it is only occupied with Co atoms. This suggests that Cu also occupies the A site because its scattering power is stronger than that of Co. In this setting the A-site cations Co^{2+} and Cu^{2+} (labeled as Co_A and Cu_A) are located at the Wyckoff position $4b(0, \frac{1}{4}, \frac{3}{8})$, while at the B-site cations Mn^{3+} and Co^{3+} ions (labeled Mn_B and Co_B) are located at $8c(0,0,0)$. The oxygen atoms occupy the position $16h(0,y,z)$, where y and z approximately have the values ~ 0.5 and ~ 0.25 ,

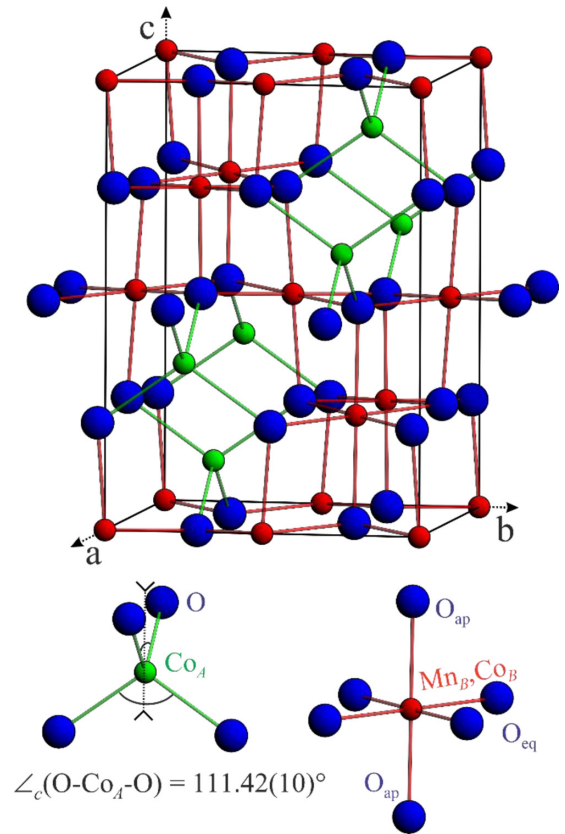


FIG. 3. Crystal structure of $\text{Mn}_{1.15}\text{Co}_{1.85}\text{O}_4$ at 3 K. In the tetragonal structure the Co_AO_4 tetrahedra show a slight compression along the c axis leading to a change from the ideal tetrahedra angle $\angle_c(\text{O}-\text{Co}_A-\text{O}) = 109.47^\circ$ to 111.42° .

respectively. The presence of Co_3O_4 and CoO leads to a reduction of the Co content in the prepared spinels giving finally the chemical compositions $(\text{Co}^{2+})_A[\text{Mn}^{3+}_{1.145(7)}\text{Co}^{3+}_{0.855(7)}]_B\text{O}_4$ and $(\text{Co}^{2+}_{0.765}\text{Cu}^{2+}_{0.235})_A[\text{Mn}^{3+}_{1.173(7)}\text{Co}^{3+}_{0.827(7)}]_B\text{O}_4$, respectively. The occupancies could be determined with good accuracy since the neutron scattering lengths of the metal atoms strongly differ, in particular for Mn which has a negative one. In the following text, we now give the formulas with the correct stoichiometry. The results of the Rietveld refinements of these two compounds are given in Table I.

It is interesting to see in Table I that the cell volume of the Cu-containing sample is slightly smaller than the undoped sample. This effect may be simply ascribed to the Cu doping at the A site since the ionic radius of Cu^{2+} ($r \sim 0.57 \text{ \AA}$) is slightly smaller than that of Co^{2+} ($r \sim 0.58 \text{ \AA}$) [47]. In fact, the Cu doping in the Co_AO_4 tetrahedra results in a slight reduction of the bond length as given in Table I. On the other hand, it can be seen in Table I that the bond lengths in the T_BO_6 octahedra are similar in both compounds. This again indicates that the Cu^{2+} ions are located at the A site. The Co^{2+} ion in the $3d^7$ configuration at the A site does not cause cooperative distortions in the CoO_4 tetrahedra through the Jahn-Teller effect. Here, the two lower-lying e_g orbitals are fully occupied with four electrons, while the higher-lying three t_{2g} orbitals are half-filled and therefore triply degenerate. On the other hand, the Jahn-Teller active Cu^{2+} ions at the A sites having the $3d^9$

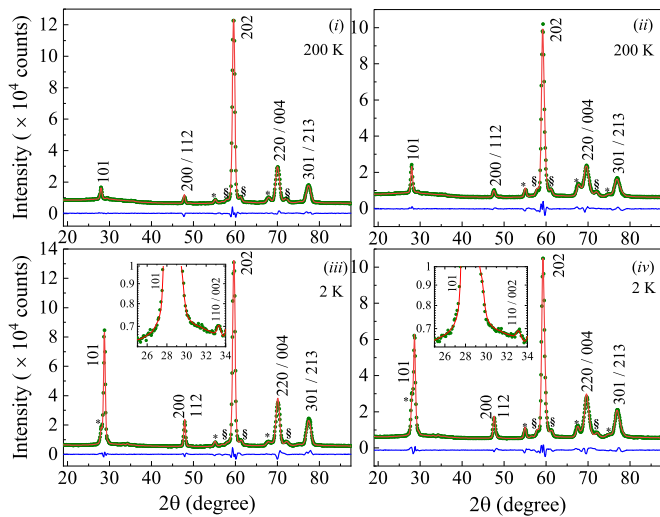


FIG. 4. Neutron powder patterns of $\text{Mn}_{1.15}\text{Co}_{1.85}\text{O}_4$ (i), (iii) and $\text{Mn}_{1.17}\text{Co}_{1.60}\text{Cu}_{0.23}\text{O}_4$ (ii), (iv) collected on the instrument E2 at 200 and 2 K, respectively. The powder patterns in the lower part of the diagram show additional magnetic intensities due to the magnetic ordering of the Mn, Co (and Cu) atoms. The insets present the prominent magnetic reflections $(101)_M$ and $(110)_M$ in enlarged form. Due to the weakness of the intensity of the reflection pair $(110)/(002)_M$ we used a logarithmic scale. The calculated (red line) and observed patterns (black open circles) as well as the difference patterns (blue line) are shown. The positions of strongest reflections of the impurities CoO and Co_3O_4 are marked with the symbols * and §, respectively.

electronic configuration leads to a decrease of the c/a ratio which is strongly established in the normal spinel CuCr_2O_4 [48]. Here, the three t_{2g} orbitals of the Cu^{2+} ions are split into one higher d_{xy} level and lower twofold-degenerate d_{xz}/d_{yz} level. But, our study showed that a Cu doping of 20 at. % does not significantly change the c/a ratio from room temperature down to 3 K (Table I). At this point it has to be noted that the strong tetragonal distortion in CuCr_2O_4 sets in concomitantly with the spontaneous onset of an orbital ordering, where a structural phase transition is observed from cubic to tetragonal [48]. This may exclude the presence of a charge ordering in the Cu-containing sample. The $T_B\text{O}_6$ octahedra contain the Jahn-Teller active ions ($T_B = \text{Mn}^{3+}$ and Co^{3+}), having the $3d^4$ and $3d^6$ configurations, respectively. For the Co^{3+} ions electronic energy can be gained if the t_{2g} levels split into a lower d_{xy} level and a higher twofold-degenerate d_{xz}/d_{yz} level. This would result in a tetragonal distortion with a $c_t/a_t\sqrt{2}$ ratio smaller than 1, and a shrinking of the apical bond $d_{ap}(T_B - \text{O})$. But, it is important to note that the tetragonal distortion could not be detected in TiCo_2O_4 [43], suggesting that the Jahn-Teller activity of the Ti^{3+} and Co^{3+} ions is rather weak or even absent in this system. A similar behavior was found for cubic Co_3O_4 , where the absence of Jahn-Teller activity of the Co^{3+} ions can be explained by a large crystal-field splitting of the $3d$ orbitals by the octahedral cubic field [45]. On the other hand, previous studies on $\text{Ti}_{0.8}\text{Mn}_{0.2}\text{Co}_2\text{O}_4$ and $\text{Ti}_{0.6}\text{Mn}_{0.4}\text{Co}_2\text{O}_4$ showed that a replacement of Ti^{3+} ions at the B site by Mn^{3+} ions leads to a weak tetragonal splitting [44]. The same trend we observe for the current compounds

$\text{Mn}_{1.15}\text{Co}_{1.85}\text{O}_4$ and $\text{Mn}_{1.17}\text{Co}_{1.60}\text{Cu}_{0.23}\text{O}_4$, where the Co^{3+} ions at the B site are replaced by Mn^{3+} ions. The crystal structure refinements of $\text{Mn}_{1.15}\text{Co}_{1.85}\text{O}_4$ and $\text{Mn}_{1.17}\text{Co}_{1.60}\text{Cu}_{0.23}\text{O}_4$ showed that the apical bond length $d_c(T_B - \text{O})$ at 3 K is slightly longer than the equatorial one $d_{ab}(T_B - \text{O})$ (Table I), while at room temperature they are practically the same. An elongation of the apical bond length $d_c(T_B - \text{O})$ would also result in an elongation of lattice parameter c giving a $c_t/a_t\sqrt{2}$ ratio larger than 1. This is contrary to the result given above, where $c_t/a_t\sqrt{2}$ ratio is weakly smaller than 1. But, it can be seen that the bond length $d_c(T_B - \text{O})$ is elongated in $\text{Mn}_{1.15}\text{Co}_{1.85}\text{O}_4$ and $\text{Mn}_{1.17}\text{Co}_{1.60}\text{Cu}_{0.23}\text{O}_4$ by only 1.84% and 1.63%, respectively. Here it is interesting to see that this small elongation does not significantly enlarge the c parameter. On the other hand, it can be seen in Fig. 3 that the bond angles $\angle_c(\text{O}-\text{A}-\text{O})$ are enlarged in the magnetically ordered range, where the angle bisector points along c . This leads to a slight shrinking of the AO_4 tetrahedra along c , which may compensate an elongation of c through the elongation of $d_c(T_B - \text{O})$. In this case the structural changes may be ascribed to magnetostriction effects. Very similar distortions were observed in $\text{Ti}_{0.8}\text{Mn}_{0.2}\text{Co}_2\text{O}_4$ and $\text{Ti}_{0.6}\text{Mn}_{0.4}\text{Co}_2\text{O}_4$ [44]. At this point it is interesting to mention that the distortion of the $T_B\text{O}_6$ octahedron is even stronger if the Mn content is increased. Therefore, we can assume that the elongation of the apical bond $d_c(T_B - \text{O})$ can be ascribed to a Jahn-Teller activity of the Mn^{3+} ions having the $3d^4$ configuration. Much stronger pronounced is this effect in Mn_3O_4 , where the bond distances are $d_{ab}(T_B - \text{O}) = 1.930(1)$ Å and $d_c(T_B - \text{O}) = 2.287(1)$ Å giving a strong elongation of 18.5% [49].

B. Magnetic ordering

In order to determine the magnetic structure, the neutron powder diffraction patterns of $\text{Mn}_{1.15}\text{Co}_{1.85}\text{O}_4$ and $\text{Mn}_{1.17}\text{Co}_{1.60}\text{Cu}_{0.23}\text{O}_4$ were collected on the instruments E2 and E6 well below and above the magnetic ordering temperature T_C . Figure 4 shows that additional magnetic intensities appearing at 2 K due to the magnetic ordering of the transition metal atoms. For both compounds the strongest magnetic intensity could be observed at the position of the 101 reflection (111 in the cubic setting) indicating a ferrimagnetic (FI) coupling between the atoms located at the A and B sites. A much weaker magnetic intensity could be observed at the position of the reflection pair 110/002 (200 in the cubic setting) indicating an additional antiferromagnetic coupling (AF) between the B atoms. For this reason, the weak reflection pair is shown in the inset of Fig. 4 in an enlarged view using a logarithmic scale. A very similar behavior could be observed for the inverse spinels TiCo_2O_4 [43] and $\text{Ti}_{1-x}\text{Mn}_x\text{Co}_2\text{O}_4$ [44], where a tetragonal splitting could not be clearly evidenced. Therefore, the magnetic structure of these spinels was described using the cubic structure with the space group $Fd\bar{3}m$. Here the B -site atoms are located at the positions (1) $0,0,0$; (2) $\frac{3}{4}, \frac{1}{4}, \frac{1}{2}$; (3) $\frac{1}{4}, \frac{1}{2}, \frac{3}{4}$; (4) $\frac{1}{2}, \frac{3}{4}, \frac{1}{4}$. It was found that the magnetic structure with the propagation vector $\mathbf{k} = 0$ is compatible with the irreducible representation (*irrep*) Γ_8 obtained from the representation analysis using the program BASIREP of the FULLPROF suite [40]. This *irrep* is of dimension 3 and it occurs two times which means that the ferromagnetic

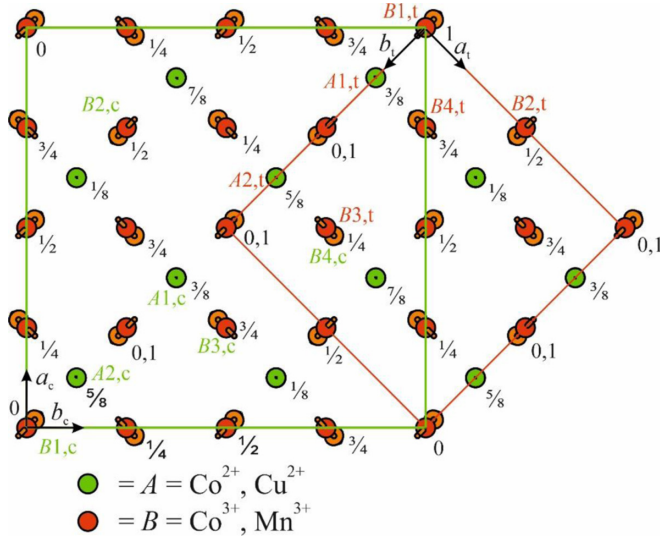


FIG. 5. Magnetic structure of $(\text{Co}^{2+})_A[\text{Mn}_{1.15}\text{Co}_{0.85}]_B\text{O}_4$ and $(\text{Co}_{0.77}\text{Cu}_{0.23})_A[\text{Mn}_{1.17}\text{Co}_{0.83}]_B\text{O}_4$. The magnetic moments of the A and B atoms are coupled ferrimagnetically along the c axis, while an antiferromagnetic noncollinear ordering of the B atoms occurs in the ab plane. In the cubic and tetragonal settings the Fourier coefficients $\mathbf{S}_k(j)$ of B atoms are the following: $\mathbf{S}_k(B1,c) = (u, u, v)$, $\mathbf{S}_k(B2,c) = (-u, -u, v)$, $\mathbf{S}_k(B3,c) = (u, -u, v)$, $\mathbf{S}_k(B4,c) = (-u, u, v)$ (cubic), and $\mathbf{S}_k(B1,t) = (0, -u, v)$, $\mathbf{S}_k(B2,t) = (0, u, v)$, $\mathbf{S}_k(B3,t) = (u, 0, v)$, $\mathbf{S}_k(B4,t) = (-u, 0, v)$ (tetragonal).

component can be aligned parallel to the axes a , b , or c . This spin structure is also compatible with the one-dimensional $irrep\Gamma_7$ derived by using the lower symmetric space group $I4_1/amd$ which also appears two times. In this setting the

B-site atoms are located at the positions (1) $0,0,0$; (2) $\frac{1}{2},0,\frac{1}{2}$; (3) $\frac{1}{4},\frac{3}{4},\frac{1}{4}$; (4) $\frac{1}{4},\frac{1}{4},\frac{3}{4}$. In contrast to the cubic setting, the ferromagnetic component is now fixed to be aligned parallel to the tetragonal c axis. Hence, the noncollinear antiferromagnetic order appears in the ab plane, where the moments point along $[110]$ and $[1\bar{1}0]$, respectively (Fig. 5). In the cubic and tetragonal settings the Fourier coefficients \mathbf{S}_k ($B1,c$) = (u, u, v) , $\mathbf{S}_k(B2,c) = (-u, -u, v)$, $\mathbf{S}_k(B3,c) = (u, -u, v)$, $\mathbf{S}_k(B4,c) = (-u, u, v)$ (cubic), and $\mathbf{S}_k(B1,t) = (0, -u, v)$, $\mathbf{S}_k(B2,t) = (0, u, v)$, $\mathbf{S}_k(B3,t) = (u, 0, v)$, $\mathbf{S}_k(B4,t) = (-u, 0, v)$ (tetragonal). A coexistence of AF and FI ordering was also observed in the orthorhombic system $\text{Ni}_{1-x}\text{Cu}_x\text{Cr}_2\text{O}_4$ [48], where the AF component is more pronounced. Here it is interesting to see that the ferrimagnetic component is also oriented along the shortest axis.

The results of the Rietveld refinements of $\text{Mn}_{1.15}\text{Co}_{1.85}\text{O}_4$ and $\text{Mn}_{1.17}\text{Co}_{1.60}\text{Cu}_{0.23}\text{O}_4$ are summarized in Table II. For both compounds the refined magnetic moment $\mu_{z,\text{FI}}(T_B)$ of the ferrimagnetically coupled B atoms varies between 1.99 and $2.12 \mu_B$. Both ions Mn^{3+} and Co^{3+} at the B site have four unpaired d electrons in the high-spin state ($3d^4$ and $3d^6$ configurations) and it can be assumed that they carry the same moment. However, the observed values are considerably smaller than the expected theoretical value of the high-spin state $\mu_{\text{eff}} = gS\mu_B = 4.0 \mu_B$. Here, it is important to note that the magnetic moment of Co^{3+} at the B site in Co_3O_4 was found to be zero, which can be explained by a large crystal-field splitting of the $3d$ orbitals by the octahedral cubic field [45,50]. The same behavior was found for the system $\text{Mn}_x\text{Co}_{3-x}\text{O}_4$, where the Mn^{3+} ions reach moment values between 3.70 and $3.83 \mu_B$ for spinels close to the composition MnCo_2O_4 [35,51,52]. Therefore, we also have set

TABLE II. Magnetic moments of the transition metal atoms in $\text{Mn}_{1.15}\text{Co}_{1.85}\text{O}_4$ and $\text{Mn}_{1.17}\text{Co}_{1.60}\text{Cu}_{0.23}\text{O}_4$ obtained from Rietveld refinements using neutron diffraction data collected on the instruments E2 and E6, respectively. In the space group $I4_1/amd$ the magnetic B^{3+} -site ions (Co^{3+} and Mn^{3+}) are located at the positions (1) $0,0,0$; (2) $\frac{1}{2},0,\frac{1}{2}$; (3) $\frac{1}{4},\frac{3}{4},\frac{1}{4}$; (4) $\frac{1}{4},\frac{1}{4},\frac{3}{4}$; the A^{2+} -site ions ($T_A^{2+} = \text{Co}^{2+}$ and Cu^{2+}) at (1) $0,\frac{1}{4},\frac{3}{8}$; (2) $0,\frac{3}{4},\frac{5}{8}$. During the refinements the moment of Co_B was set equal to zero. In addition to the individual moments $\mu(\text{Mn})$ the averaged moments at the T site are also listed. The resulting ferromagnetic moments $2\mu_{z,\text{FI}}(T_B) - \mu_{z,\text{FI}}(T_A)$ are compared with the spontaneous magnetizations M measured at 2 K and the theoretical moment values. For the analysis of the E6 data the small moment $\mu_{xy,\text{AF}}$ (determined from E2 data) was not allowed to vary. The obtained moment values of $\text{Mn}_{1.15}\text{Co}_{1.85}\text{O}_4$ are compared with those given earlier in Refs. [51,52], where the Mn content is slightly larger.

	$\text{Mn}_{1.15}\text{Co}_{1.85}\text{O}_4$ E2 (at 1.7 K)	$\text{Mn}_{1.15}\text{Co}_{1.85}\text{O}_4$ E6 (at 1.9 K)	$\text{Mn}_{1.2}\text{Co}_{1.8}\text{O}_4$ Ref. [51] ^a	$\text{Mn}_{1.22}\text{Co}_{1.78}\text{O}_4$ Ref. [52]	$\text{Mn}_{1.17}\text{Co}_{1.60}\text{Cu}_{0.23}\text{O}_4$ E2 (at 1.7 K)	$\text{Mn}_{1.17}\text{Co}_{1.60}\text{Cu}_{0.23}\text{O}_4$ E6 (at 1.9 K)
$\mu_{z,\text{FI}}(T_A)$ (μ_B)	3.04(3)	3.11(3)	3.09	3.03(5)	2.25(4)	2.35(3)
$\mu_{z,\text{FI}}(\text{Mn}_B)$ (μ_B)	3.51(5)	3.40(6)	3.70	3.83(8)	3.64(5)	3.70(6)
$\mu_{xy,\text{AF}}(\text{Mn}_B)$ (μ_B)	0.55(8)	0.55			0.55(8)	0.55
$\mu_{\text{tot}}(\text{Mn}_B)$ (μ_B)	3.56(6)	3.45(6)			3.68(6)	3.74(6)
$\mu_{z,\text{FI}}(T_B)$ (μ_B)	2.06(3)	1.99(4)	2.22	2.34(4)	2.08(3)	2.12(4)
$\mu_{xy,\text{AF}}(T_B)$ (μ_B)	0.32(6)	0.32			0.31(6)	0.31
$\mu_{\text{tot}}(T_B)$ (μ_B)	2.08(3)	2.02(3)			2.10(3)	2.14(3)
$2\mu_{z,\text{FI}}(T_B)$ (μ_B)	4.12(5)	3.99(7)	4.44	4.67(9)	4.17(5)	4.24(7)
R_M/R_F	0.0266/0.0116	0.0481/0.0127			0.0387/0.0261	0.0208/0.0120
$2\mu_{z,\text{FI}}(T_B) - \mu_{z,\text{FI}}(T_A)$ (μ_B)	1.08(8)	0.88(10)	1.35	1.64	1.92(9)	1.89(10)
μ (μ_B) [§]	0.89–1.13	0.89–1.13	1.20(5)	1.09	0.97–1.21	0.97–1.21
$\mu(T_A)$ (μ_B) ^b	3.0	3.0			2.3	2.3
$\mu(T_B)$ (μ_B) ^b	2.3	2.3			2.34	2.34

^aStandard deviations or error bars were not given for all moment values in the literature, § up to $H = 90$ kOe.

^bTheoretical value for spin-only moment.

the moment of Co^{3+} to zero during the refinements. Finally, slightly smaller moments $\mu_{z,\text{FI}}(\text{Mn}_B)$ have been deduced for $\text{Mn}_{1.15}\text{Co}_{1.85}\text{O}_4$ varying between 3.40 and $3.51 \mu_B$. It can be pointed out here that an AF component could not be found in earlier studies. An AF ordering additionally generates magnetic intensity on the reflection (111), in our case about 13% of the total intensity, whereas the magnetic intensity of the reflection pair (110)/(002) (200 in the cubic setting) is relatively weak. For both $\text{Mn}_{1.15}\text{Co}_{1.85}\text{O}_4$ and $\text{Mn}_{1.17}\text{Co}_{1.60}\text{Cu}_{0.23}\text{O}_4$ the AF moment is $\mu_{xy,\text{AF}}(\text{Mn}_B) = 0.55(8) \mu_B$, or the averaged moment $\mu_{xy,\text{AF}}(T_B) = 0.32(8) \mu_B$. If this AF component is not taken into account, then the FI moment results in an enlarged value. This explains why the B -site moments, given in Refs. [35,51,52], were found to be larger than those determined in our study. In total, the Mn moments reach the values $\mu_{\text{tot}}(\text{Mn}_B) = 3.45 - 3.56 \mu_B$ ($\text{Mn}_{1.15}\text{Co}_{1.85}\text{O}_4$) and $\mu_{\text{tot}}(\text{Mn}_B) = 3.68 - 3.74 \mu_B$ ($\text{Mn}_{1.17}\text{Co}_{1.60}\text{Cu}_{0.23}\text{O}_4$), respectively. These are in good agreement with the value $3.55 \mu_B/\text{Mn}^{3+}$ as found earlier for Mn_3O_4 [53]. This also indicates that Co^{3+} does not contribute to the magnetic order in these spinels. On the other hand, it is interesting to see that the Co^{3+} ions in TiCo_2O_4 carry a moment of about $2 \mu_B$ [43], where Ti^{3+} and Co^{3+} occupy the B site. For the compound $\text{Ti}_{0.6}\text{Mn}_{0.4}\text{Co}_2\text{O}_4$ [or in detail $\text{Co}(\text{Ti}_{0.3}\text{Mn}_{0.2}\text{Co}_{0.5})_2\text{O}_4$] the averaged moment value at the B site varies between 2.25 and $2.48 \mu_B$. If the moment of Mn^{3+} is fixed to be $3.84 \mu_B$ the Co^{3+} ion moment varies between 1.2 and $1.4 \mu_B$. For this calculation the constraint $\mu(\text{Mn}^{3+}) = 4 \times \mu(\text{Ti}^{3+})$ was used [44]. These observations show a trend that the Co moment in these spinels is decreasing with increasing Mn content resulting possibly in a reduction of the crystal-field splitting of the $3d$ orbitals of Co^{3+} by the octahedral cubic field.

The magnetic moment of the Co^{2+} ion at the A site reaches the values between 3.04 and $3.11 \mu_B$ in $\text{Mn}_{1.15}\text{Co}_{1.85}\text{O}_4$ which are in a very good agreement with $3.08 \mu_B$ given in Ref. [51]. The experimental moments practically reach the theoretical value $\mu_{\text{eff}} = gS \mu_B = 3.0 \mu_B$ of the high-spin state of Co^{2+} ion which has three unpaired electrons in the $3d^7$ configuration. In contrast, the A -site magnetic moment varies between 2.25 and $2.35 \mu_B$ for $\text{Mn}_{1.17}\text{Co}_{1.60}\text{Cu}_{0.23}\text{O}_4$. This result can be ascribed to the smaller moment of the Cu^{2+} ions which replace 20 at. % of the Co^{2+} ions at the A site. In the $3d^9$ configuration these ions only have one unpaired electron giving the expected theoretical value in the high-spin state $\mu_{\text{eff}}(\text{Cu}^{2+}) = gS \mu_B = 1.0 \mu_B$. Therefore, one obtains the theoretical moment $\mu_{\text{eff}}(\text{Co}^{2+}/\text{Cu}^{2+}) = gS \mu_B = 2.6 \mu_B$. Here the presence of a spin-orbital coupling is not taken into account. Nevertheless, we have tried to estimate the individual moment values at the A site using the constraint $\mu(\text{Co}^{2+}) = 3 \times \mu(\text{Cu}^{2+})$. In this way, for the experimental moments which vary between 2.25 and $2.35 \mu_B$ the individual moments are estimated to differ as follows: between 2.60 and $2.71 \mu_B$ for Co^{2+} , between 0.87 and $0.90 \mu_B$ for Cu^{2+} , respectively.

Thermal variation of the magnetic moments of cations located at the A and B sites for both the compositions are shown in Fig. 6 inferring the dominant ferrimagnetic (FI) coupling. Due to the different moment values at the A and B sites one obtains a resultant FI moment which is defined as $2\mu_{\text{FI}}(T_B) - \mu_{\text{FI}}(T_A)$ ($T_A = \text{Co}_A$ and Cu_A , $T_B = \text{Mn}_B$ and

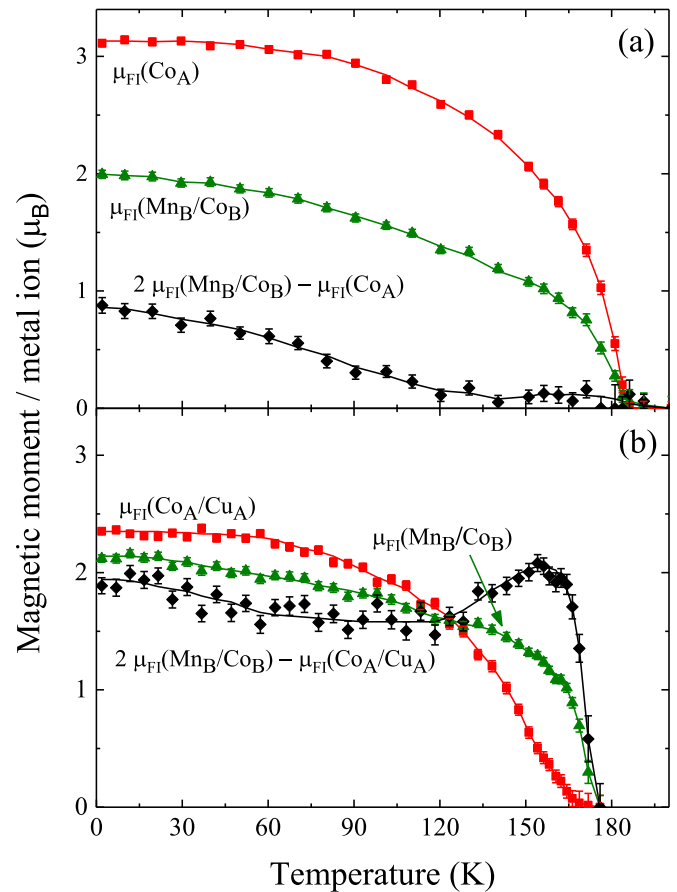


FIG. 6. Temperature dependence of the experimental magnetic moments of the ions in (a) $\text{Mn}_{1.15}\text{Co}_{1.85}\text{O}_4$ and (b) $\text{Mn}_{1.17}\text{Co}_{1.60}\text{Cu}_{0.23}\text{O}_4$ located at the A and B sites. The A site is occupied with Co^{2+} (and Cu^{2+}) ions [labeled as Co_A (and Cu_A)], while the B site contains Mn^{3+} and Co^{3+} (labeled as Mn_B and Co_B). Also shown is the thermal variation difference moment of the two ferromagnetic sublattices according to the expression $2\mu_{\text{FI}}(\text{Co}_B/\text{Mn}_B) - \mu_{\text{FI}}(\text{Co}_A/\text{Cu}_A)$. The bold lines are a guide for the eye.

Co_B). Also, we have estimated theoretically the individual site moments for both compounds on the basis of the observed cation distribution and spin-only moment, which are given in Table II. One can notice that the A -sublattice moment (determined from neutron data) is consistent with theoretical value for both compound, on the other hand, the B -sublattice moment shows reduced value compared to theoretical one. Such decrease of the B -sublattice moment can be ascribed to frustration effects in the kagome lattice consisting of B atoms. The insets of Figs. 4(iii) and 4(iv) show the enlarged view around the base of 101 neutron-diffraction peak of both the compositions at 2 K revealing the presence of diffuse scattering close to the reflection pair (110)/(002). Such well-resolved satellite Bragg reflections usually originate from the disordered transverse spin components (TSC), indicating the presence of canted local spin configuration on the B sublattice similar to the Yafet-Kittel's (YK) three-sublattice structure [54,55]. Accordingly, we have evaluated the canting angle (α_{YK}) using the measured individual site moments

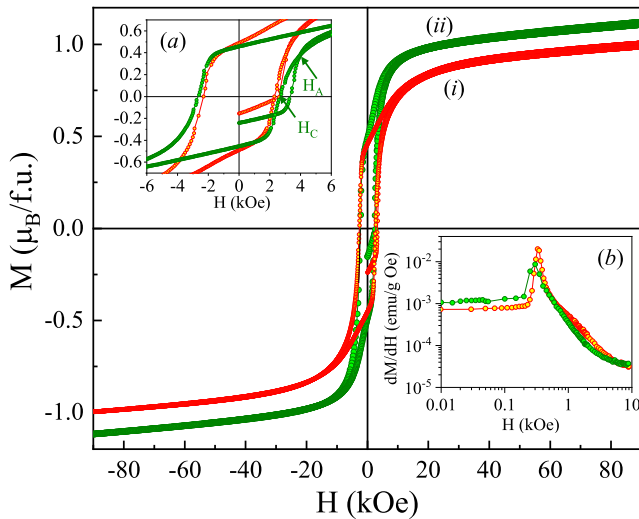


FIG. 7. Magnetic field dependencies of magnetization $M(H)$ of (i) $\text{Mn}_{1.15}\text{Co}_{1.85}\text{O}_4$ (red) and (ii) $\text{Mn}_{1.17}\text{Co}_{1.60}\text{Cu}_{0.23}\text{O}_4$ (green) measured at 1.9 K under zero-field-cooled condition. The inset (a) shows the magnified region of $M(H)$ curve to highlight anisotropy field (H_A) and (b) represents the first derivatives $dM/dH(H)$ for both samples.

and total magnetic moments derived from the Bragg's reflections for both the compositions. Subsequently, at $T = 1.7$ K, we obtained the magnitude of $\alpha_{\text{YK}} = 28^\circ$ and 25° for pristine and Cu-substituted spinels, respectively. Such noncollinear arrangement of spins results to substantial decrease of the magnitude of B -sublattice moments than the expected value as noticed from Fig. 6 ($2.35 - 2.16 \mu_B$) instead of theoretical moment $5.65 \mu_B$. Usually, the transverse spin-glass component (often called "semi-spin-glass") coexists with the longitudinal-spin component (LSC) when the magnetic ions are diluted with nonmagnetic or less magnetic ions (such as Cu in the present case). Such noncollinear spin arrangement can also be found in other spinel oxides diluted with less magnetic cations [56,57]. The canted spin arrangement weakens the A - B exchange interactions and reduces saturation magnetization. Such unsaturated feature is clearly noticeable from the low-temperature magnetic hysteresis curve which measured at 2 K up to very high field 9 T (Fig. 7). The temperature dependence of the net magnetization curve of $\text{Mn}_{1.17}\text{Co}_{1.60}\text{Cu}_{0.23}\text{O}_4$ sample shows a maximum around 150 K. We assume such anomaly comes due to the following three reasons: (i) different crystal-field environments and dissimilar exchange interaction created due to Cu doping. (ii) Anisotropy plays a key role which leads to different temperature dependence of magnetic moments. (iii) Another possibility is that the moments of one sublattice decrease faster than those of the other one which leads to an increase of the ferrimagnetic moment but this might be independent from the temperature dependence of the antiferromagnetic part. Moreover, recent studies by Garlea *et al.* reported the existence of two transitions to long-range-ordered ferromagnetic states, the first collinear (ferri-paramagnetic) and the second noncollinear ferrimagnetic ordering within the orbitally ordered tetragonal phase of spinel MnV_2O_4 [58,59]. In this system the low- T transition is characterized by the

growth of AFM components in the basal plane, is accompanied by a tetragonal distortion and the appearance of a gap in the magnetic excitation spectrum [58]. We expect that the above-described noncollinear uncompensated complicated spin structure may exist in the present systems although these compounds are not completely isostructural to the vanadate spinels.

We also studied the change of the peak shape of magnetic reflection $(101)_M$ as a function of temperature. For both the compositions, the magnetic reflection shows the same peak shape as the nuclear reflections. In contrast, a pure Lorentzian peak shape has been observed for the other spinel TiCo_2O_4 in the full temperature range [43]. For this compound, a strong contribution of diffuse scattering has been observed previously giving an uneven background. On the other hand, a change from a Gaussian into a Lorentzian peak shape with increasing temperature could be observed for Ti-diluted systems such as $\text{Ti}_{0.6}\text{Mn}_{0.4}\text{Co}_2\text{O}_4$ and $\text{Ti}_{0.2}\text{Mn}_{0.8}\text{Co}_2\text{O}_4$ [44].

C. Magnetization and magnetic resonance measurements

Figure 7 represents the magnetization versus field (M - H) hysteresis loops for both the compositions $\text{Mn}_{1.15}\text{Co}_{1.85}\text{O}_4$ and $\text{Mn}_{1.17}\text{Co}_{1.60}\text{Cu}_{0.23}\text{O}_4$ measured at 1.9 K under the zero-field-cooled (ZFC) condition. From the graph it can be observed that 20 at.% of Cu-doped sample shows higher magnetization as compared to the undoped case. Such increase in the net magnetization ($\mu_N = M_{\text{Mn}} - M_{\text{Co/Cu}}$) for $T < T_C$ is due to the presence of low moment Cu^{2+} cations at the tetrahedral A sites which replace the Co spins and are oppositely aligned with octahedral Mn spins. A close observation of these loops indicates that the initial magnetic curves lie outside the hysteresis loops, and the anisotropy field (H_A) is larger than coercive field (H_C). It is interesting to note that the initial magnetic curves meet the main loops only at very high fields which can also be seen from the first derivative of $M(H)$ curves (known as field-induced transition H_D) which suggest the reorientation of magnetic domains towards the externally applied magnetic fields. H_D value decreases from 4.0 to 3.1 kOe for 20% of Cu-substituted sample. Similar behavior was reported by Joy and Date for a MnCo_2O_4 polycrystalline sample [26]. They observe that the stiffness of the domain wall motion remains up to a very high temperature ~ 130 K and predicted direct correlation between domain structure and the shapes of magnetization curve at low fields. Furthermore, it can be seen from the $M(H)$ graph that the magnetization is not saturated even by applying high fields up to ± 90 kOe, which represents the noncollinear arrangement of spins. The angle of the spins changes due to the torque exerted by the magnetic field, leading to a linear increase in the magnetization value with increasing the field within the magnetically ordered state. So in order to obtain the approximate magnitude of the saturation magnetization (M_S) we plotted the variation of M as a function of $1/H$ (inset of Fig. 8) and obtained the value of M_S (for H_{DC} until 90 kOe) by the linear extrapolation method ($H^{-1} \rightarrow 0$). Consequently, the M_S value (~ 1.07 and $1.22 \mu_B/f.u.$ for $\text{Mn}_{1.15}\text{Co}_{1.85}\text{O}_4$ and $\text{Mn}_{1.17}\text{Co}_{1.60}\text{Cu}_{0.23}\text{O}_4$) obtained at 1.9 K (ordered region) represents the net magnetization of A and B sublattices which are coupled antiparallel to each other through strong A - O - B exchange interactions.

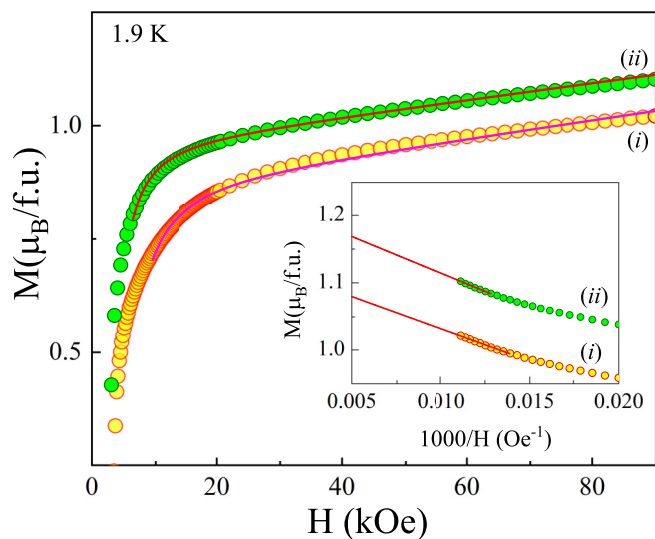


FIG. 8. Isothermal magnetization (M - H) curves of (i) $\text{Mn}_{1.15}\text{Co}_{1.85}\text{O}_4$ (red) and (ii) $\text{Mn}_{1.17}\text{Co}_{1.60}\text{Cu}_{0.23}\text{O}_4$ (green) recorded at 1.9 K and fitted with the law-of-approach-to-saturation (LAS) expression. Circular points represent the experimentally obtained data and the straight line corresponds to the best fits corresponding to the LAS equation to the experimental data. The inset shows inverse magnetic field dependence of magnetization $M(H^{-1})$ measured at 1.9 K. The straight line corresponds to the best fit.

For both systems the net magnetic moment (μ) calculated from $\mu = N_A g S M_S$ confirms the presence of high-spin state of Co^{2+} ($S = \frac{3}{2}$) and Mn^{3+} ($S = 2$) and is comparable to magnetic moment value obtained from the neutron diffraction analysis as discussed in the previous section. On the other hand, the magnetocrystalline anisotropy present in these systems can be determined using the law of approach to saturation (LAS) method by fitting the below expression with the M - H data for $H > H_C$ near the magnetic saturation [60]: $M = M_S[1 - A/H - B/H^2] + \chi H$. In this expression the constant A represents the contributions from microstress, whereas $B(= 8K_U^2/105\mu_0^2M_S^2)$ signifies the contribution of magnetocrystalline anisotropy (MCA) and the component χH is known as forced magnetization. Accordingly, the solid lines shown in Fig. 8 represent the best fit to the M - H isotherm with the LAS equation which yields anisotropy constant $K_U = 9 \times 10^5$ and 7.5×10^5 erg/cm³ for $\text{Mn}_{1.15}\text{Co}_{1.85}\text{O}_4$ and $\text{Mn}_{1.17}\text{Co}_{1.60}\text{Cu}_{0.23}\text{O}_4$, respectively. Also, the presence of high MCA of samples is further supported by the $\chi_{dc}(T)$ data where we noticed a giant irreversible bifurcation between $\chi_{dc\text{-ZFC}}(T)$ and $\chi_{dc\text{-FC}}(T)$. Figures 9(a)–9(c) show the thermal variation of dc-magnetic susceptibility χ_{dc} (left-hand-side scale) recorded under field-cooled condition (at $H = 1$ kOe), ac-magnetic susceptibility χ_{ac} (right-hand-side scale) measured at zero dc-magnetic field and constant ac-peak-to-peak amplitude of magnetic field $h_{ac} \sim 3$ Oe with frequency $\omega \sim 10$ Hz and specific heat C_p . Accordingly, the magnetic ordering temperatures $T_C \sim 184$ and 164 K of $\text{Mn}_{1.15}\text{Co}_{1.85}\text{O}_4$

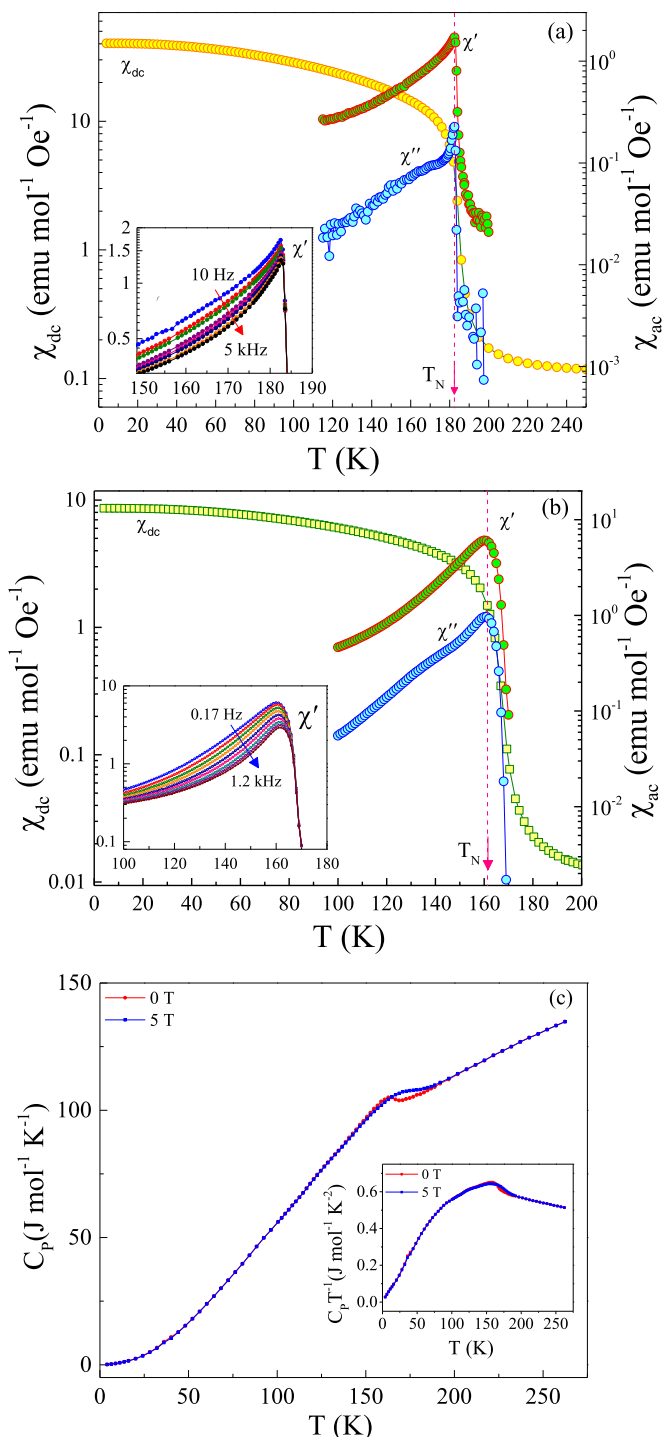


FIG. 9. Temperature dependence of dc-magnetic susceptibility $\chi_{dc}(T, H_{dc} = 1$ kOe) (left-hand-side scale) along with the real and imaginary components $\chi'(\omega)$ and $\chi''(\omega)$ of the ac-magnetic susceptibility $\chi_{ac}(T, \omega, H_{dc} = 0$ Oe) (right-hand-side scale) for (a) $\text{Mn}_{1.15}\text{Co}_{1.85}\text{O}_4$ and (b) $\text{Mn}_{1.17}\text{Co}_{1.60}\text{Cu}_{0.23}\text{O}_4$, respectively. The insets in (a) and (b) show the frequency dependency of the real component $\chi'(\omega)$. (c) Temperature variation of the specific heat $C_p(T)$ of $\text{Mn}_{1.17}\text{Co}_{1.60}\text{Cu}_{0.23}\text{O}_4$ measured under both zero magnetic field (H) (red color) and $H = 50$ kOe (blue color). The inset shows the low-temperature region of $C_p T^{-1}$ versus T .

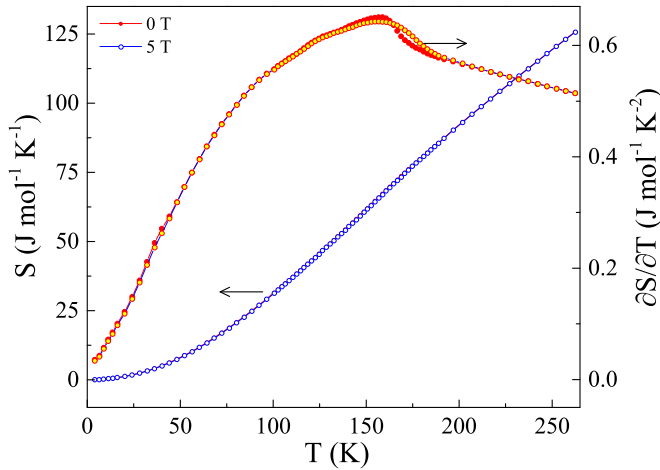


FIG. 10. Temperature dependence of the entropy $S(T)$ of $\text{Mn}_{1.17}\text{Co}_{1.60}\text{Cu}_{0.23}\text{O}_4$ system obtained from the heat-capacity data for both $H = 0$ and 50 kOe. The temperature dependence of differential entropy $\partial S/\partial T$ is depicted on the right-hand-side scale which clearly shows the hump across the ordering temperature.

and $\text{Mn}_{1.17}\text{Co}_{1.60}\text{Cu}_{0.23}\text{O}_4$ are obtained from the $\chi_{ac}(T)$, $\chi_{dc}(T)$, and $C_p(T)$ data which are in good agreement with the temperature dependence of site-specific cation magnetic moments from the neutron diffraction data as discussed above. Although there is a weak frequency dispersion of the peak position in both real and imaginary components of the $\chi_{ac}(T)$ data [inset of Figs. 9(a) and 9(b)] we did not notice any signatures of glassy characteristics using either power-law or Vogel-Fulcher laws. These results are in line with the variation of $C_p(T)$ plots for $\text{Mn}_{1.17}\text{Co}_{1.60}\text{Cu}_{0.23}\text{O}_4$ where we did not notice a sharp transition across the T_C usually obtained in any antiferromagnetic, ferrimagnetic, or ferromagnetic system because of the broad and weak ferrimagnetic ordering of the system. The order-to-disorder transition in heat-capacity data further smears in the presence of externally applied magnetic field of 50 kOe wherein a broad hump at 165 K noticed for $H = 0$ Oe is shifted towards the high-temperature side with significant drop in the magnetization. Similar features are observed in case of temperature dependence of entropy (dS/dT) plots (Fig. 10) obtained from the $C_p(T)$ data signifying the loss of entropy to the magnetic domains consisting of weakly correlated ferrimagnetic spins.

In order to probe magnetic transition driven by the domain orientation and the magnetocrystalline anisotropy of the investigated samples, we performed the ferromagnetic resonance (FMR) absorption spectra at different temperatures. Figure 11 shows the FMR absorption spectra of $\text{Mn}_{1.15}\text{Co}_{1.85}\text{O}_4$ and $\text{Mn}_{1.17}\text{Co}_{1.60}\text{Cu}_{0.23}\text{O}_4$ polycrystalline samples recorded at different temperatures using the X-band microwave radiation of frequency 9.8 GHz. The temperature evolution of magnetic transitions for both samples is determined by calculating the absorption intensity of each spectrum. We analyzed the absorption spectra by calculating the resonance field, and the resonance linewidth ΔH , which will play a key role for the further analysis. For polycrystalline samples the resonance spectrum includes the contribution of the absorption lines of the crystallites oriented in all the possible space directions

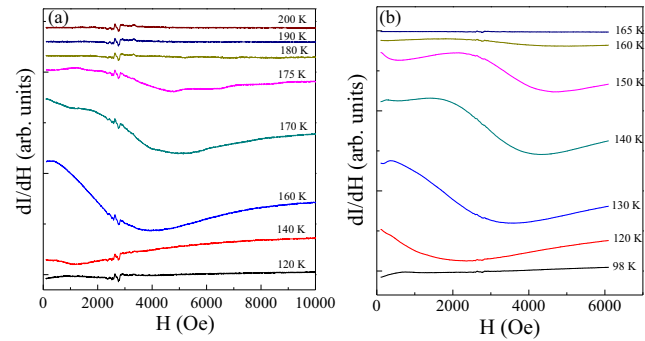


FIG. 11. The first derivative of X-band FMR spectral intensity (dI/dH) versus field (H) for $\text{Mn}_{1.15}\text{Co}_{1.85}\text{O}_4$ (a) and $\text{Mn}_{1.17}\text{Co}_{1.60}\text{Cu}_{0.23}\text{O}_4$ (b) recorded at different temperatures between 100 and 200 K.

relative to the magnetic field. The temperature dependence of absorption intensity is determined by multiplying the observed linewidth by the FMR intensity at resonance and is shown in Fig. 12. The main features observed in the temperature evolution of the FMR intensity can be summarized as follows: (i) At low temperature, the FMR intensity is low because of high anisotropy and coercive field present in the sample, which corresponds to the considerable resistance to the domain wall motion. Such resistance on domain wall motion can be found up to a very high temperature from the hysteresis data discussed above. (ii) As the temperature increases, the coercive field as well as the anisotropy field decrease and domain walls start to reorient at a critical resonance field. (iii) With further increasing temperature, the FMR intensity increases up to a maximum and abruptly decreases

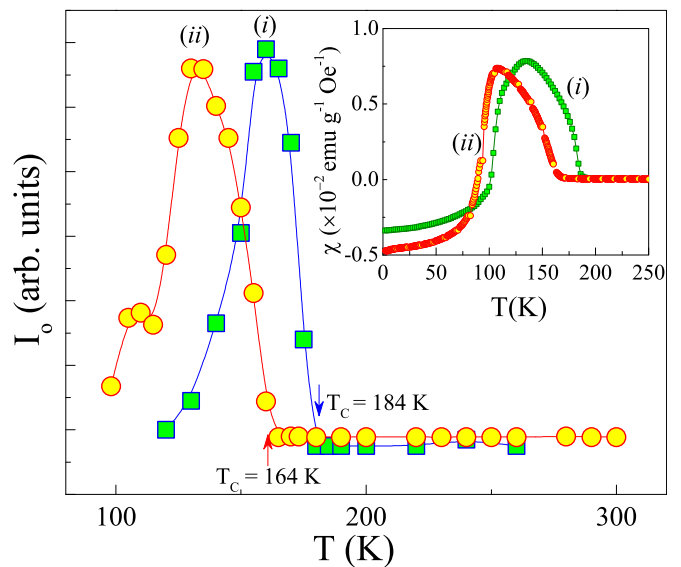


FIG. 12. The temperature dependence of integrated intensity (I_0) of the FMR spectra for both polycrystalline compounds (i) $\text{Mn}_{1.15}\text{Co}_{1.85}\text{O}_4$ (green) and (ii) $\text{Mn}_{1.17}\text{Co}_{1.60}\text{Cu}_{0.23}\text{O}_4$ (red). Inset shows the $\chi(T)$ of $\text{Mn}_{1.15}\text{Co}_{1.85}\text{O}_4$ (green) and $\text{Mn}_{1.17}\text{Co}_{1.60}\text{Cu}_{0.23}\text{O}_4$ (red) measured under ZFC conditions in the presence of external dc-magnetic field of 1 kOe. The arrow marks represent the ferrimagnetic ordering temperature T_C .

to lower value. Such decrease of FMR intensity suggests the presence of internal fields which are proportional to the spontaneous magnetization that increases rapidly close to T_C . Also, it is interesting to see that there is a close resemblance between the temperature dependence of FMR intensity and the temperature dependence of magnetic susceptibility $\chi(T)$ (inset of Fig. 12). Such similarity between FMR intensity and χ can also be found in other systems [60,61]. Comparing both results, one can say the suppression of FMR intensity suggests the magnetic ordering temperature across $T_C \sim 184$ and 164 K for $\text{Mn}_{1.15}\text{Co}_{1.85}\text{O}_4$ and $\text{Mn}_{1.17}\text{Co}_{1.60}\text{Cu}_{0.23}\text{O}_4$, respectively, and the presence of high magnetocrystalline anisotropy at low temperature.

IV. CONCLUSIONS

In conclusion, we have studied in detail the structural and magnetic properties of a polycrystalline sample of $\text{Mn}_{1.15}\text{Co}_{1.85}\text{O}_4$ and $\text{Mn}_{1.17}\text{Co}_{1.60}\text{Cu}_{0.23}\text{O}_4$ by x-ray and neutron diffraction, FMR, magnetization, and heat-capacity measurements. The crystal structure of both the systems is found to be tetragonal with the space group $I4_1/amd$. The crystal structure refinements reveal that the apical bond length $d_c(T_B\text{-O})$ is slightly longer than the equatorial bond length $d_{ab}(T_B\text{-O})$ for both the compounds due to the Jahn-Teller active Mn^{3+} ions. Our results demonstrated that both the compounds exhibit weak tetragonal distortion with a c/a ratio smaller than 1 which may be ascribed to ionic-size effects. The refinements of the neutron data also allowed us to determine precisely the following cationic distribution: $(\text{Co}^{2+})_A[\text{Mn}_{1.148(7)}^{3+}\text{Co}_{0.852(7)}^{3+}]_B\text{O}_4$ and $(\text{Co}_{0.765}^{2+}\text{Cu}_{0.235}^{2+})_A[\text{Mn}_{1.173(7)}^{3+}\text{Co}_{0.827(7)}^{3+}]_B\text{O}_4$. These results clearly show that Cu^{2+} replaces the Co^{2+} ions at the A site driving finally the exchange interactions between the magnetic moments at the A and B sites. For example, in the system $\text{Cu}_{1-x}\text{Zn}_x\text{Cr}_2\text{O}_4$ a substitution of Cu^{2+} with even non-magnetic Zn^{2+} creates a strong increase of coercive fields which can be ascribed to a freezing effect of the local anisotropy [62]. The neutron diffraction and magnetization data as well as the temperature dependence of FMR spectra confirmed a ferrimagnetic ordering in both $\text{Mn}_{1.15}\text{Co}_{1.85}\text{O}_4$ and $\text{Mn}_{1.17}\text{Co}_{1.60}\text{Cu}_{0.23}\text{O}_4$ below 184 and 164 K, respectively. In our study we were able to find out that the coupled B site moments are aligned parallel to the c axis, while a weak noncollinear antiferromagnetic spin order occurs in the ab plane. The low-temperature hysteresis analysis reveals high magnetocrystalline anisotropy $K_U (\sim 9 \times 10^5 \text{ erg/cm}^3)$ for both samples. These results are complemented with the

temperature dependence of magnetization data, where a giant bifurcation is evident between the $M_{\text{ZFC}}(T)$ and $M_{\text{FC}}(T)$. Interestingly, both the systems exhibit a field-induced transition across H_D (~ 4.0 kOe) which is associated with the domain reorientation. The ordering temperature determined from the heat-capacity data and $\chi_{\text{ac}}(T)$ and $\chi_{\text{dc}}(T)$ are in good agreement with the neutron diffraction data. The absence of sharp transition in $C_P(T)$ corroborates with the inadequate frequency dispersion of the cusp $T_C(\omega)$ in $\chi_{\text{ac}}(T)$ collectively signifying the fact that the investigated system consists of weakly coupled ferrimagnetic spins. Moreover, the use of different methods is necessary to give a detailed description of the structural and magnetic properties of this system. X-ray and neutron scattering data revealed important details about the structural properties of $\text{Mn}_{1.15}\text{Co}_{1.85}\text{O}_4$ and $\text{Mn}_{1.17}\text{Co}_{1.60}\text{Cu}_{0.23}\text{O}_4$, especially the change of the crystal structure symmetry which is related to the ionic-size or/and Jahn-Teller effect. Atomic positions of the magnetic ions are fundamental for the accurate interpretation of the magnetic properties of this system which has been revealed by the current studies. Further, this study concludes that the knowledge of the precise crystal structure is essential to determine the magnetic structure in detail which is strongly correlated with each other. Especially, the discovery of the additional antiferromagnetic components lying in the ab plane is necessary to describe the magnetization processes, and such aspects were not previously known in this material. This leads to additional interactions between the antiferromagnetic and ferrimagnetic sublattices due to which an exchange-bias effect along with the increasing coercive field becomes obvious. It is also a significant part to drive the change of structural and magnetic properties by partial substitution of the Cu atoms as done in this work for $\text{Mn}_{1.17}\text{Co}_{1.60}\text{Cu}_{0.23}\text{O}_4$. The FMR and bulk magnetic measurements give additional information about magnetocrystalline anisotropy and field-induced effects of the system. Further theoretical and application-based studies on the investigated system will promote the development of oxide-based spintronic devices.

ACKNOWLEDGMENTS

P.P. acknowledges the FIST programme of Department of Science and Technology, India for partial support of this work (Grants No. SR/FST/PSII-020/2009 and No. SR/FST/PSII-037/2016). J. G. Lin acknowledges the support by the Ministry of Science and Technology of R. O. C. under the projects of MOST Grant No. 109-2112-M-002-006. We thank R. Feyerherm for performing x-ray diffraction experiments.

-
- [1] A. Ramirez, *Annu. Rev. Mater. Sci.* **24**, 453 (1994).
 [2] C. Urano, M. Nohara, S. Kondo, F. Sakai, H. Takagi, T. Shiraki, and T. Okubo, *Phys. Rev. Lett.* **85**, 1052 (2000).
 [3] N. Tristan, J. Hemberger, A. Krimmel, H.-A. Krug von Nidda, V. Tsurkan, and A. Loidl, *Phys. Rev. B* **72**, 174404 (2005).

- [4] M. Thackeray, W. David, P. Bruce, and J. Goodenough, *Mater. Res. Bull.* **18**, 461 (1983).
 [5] K. H. Lee, H. Chang, I. Y. Hwang, J.-H. Chung, H. W. Kang, S. J. Kim, and S. Lee, *Phys. Rev. B* **91**, 064404 (2015).
 [6] Y. Chen, X.-Y. Zhang, C. Vittoria, and V. Harris, *Appl. Phys. Lett.* **94**, 102906 (2009).

- [7] Q. Zhang, K. Singh, F. Guillou, C. Simon, Y. Breard, V. Caignaert, and V. Hardy, *Phys. Rev. B* **85**, 054405 (2012).
- [8] D. P. Shoemaker, E. E. Rodriguez, R. Seshadri, I. S. Abumohor, and T. Proffen, *Phys. Rev. B* **80**, 144422 (2009).
- [9] R. Zheng, G. Wen, K. Fung, and X. Zhang, *J. Appl. Phys.* **95**, 5244 (2004).
- [10] Y. Muraoka, H. Tabata, and T. Kawai, *Appl. Phys. Lett.* **77**, 4016 (2000).
- [11] K. Tomiyasu, J. Fukunaga, and H. Suzuki, *Phys. Rev. B* **70**, 214434 (2004).
- [12] J. Hubsch and G. Gavoille, *Phys. Rev. B* **26**, 3815 (1982).
- [13] P. Pramanik, S. Singh, M. R. Chowdhury, S. Ghosh, V. Sathe, K. M. Rabe, D. Vanderbilt, M. S. Seehra, and S. Thota, *Phys. Rev. B* **104**, 014433 (2021).
- [14] P. Pramanik, S. Ghosh, P. Yanda, D. C. Joshi, S. Pittala, A. Sundaresan, P. K. Mishra, S. Thota, and M. S. Seehra, *Phys. Rev. B* **99**, 134422 (2019).
- [15] Y. Kwak, J. Song, and T. Koo, *J. Korean Phys. Soc.* **69**, 263 (2016).
- [16] H. Chang, I.-Y. Hwang, J.-H. Chung, J. R. Stewart, W. Higemoto, and Y. Miyake, *Phys. Rev. B* **97**, 014406 (2018).
- [17] V. Tsurkan, S. Zherlitsyn, S. Yasin, V. Felea, Y. Skourski, J. Deisenhofer, H.-A. Krug von Nidda, J. Wosnitza, and A. Loidl, *Phys. Rev. Lett.* **110**, 115502 (2013).
- [18] Y. Yang, Y. Zhao, L. Xiao, and L. Zhang, *Electrochem. Commun.* **10**, 1117 (2008).
- [19] L. Li, Y. Zhang, X. Liu, S. Shi, X. Zhao, H. Zhang, X. Ge, G. Cai, C. Gu, X. Wang *et al.*, *Electrochim. Acta* **116**, 467 (2014).
- [20] L. Li, G. Jiang, and J. Ma, *Mater. Res. Bull.* **104**, 53 (2018).
- [21] Z. Li, X. Huang, J. Hu, A. Stein, and B. Tang, *Electrochim. Acta* **247**, 1 (2017).
- [22] H. Wang, Y. Yang, Y. Liang, G. Zheng, Y. Li, Y. Cui, and H. Dai, *Energy Environ. Sci.* **5**, 7931 (2012).
- [23] S. Sahoo, K. K. Naik, and C. S. Rout, *Nanotechnology* **26**, 455401 (2015).
- [24] S. Shibli, P. Arun, and A. V. Raj, *RSC Adv.* **5**, 19393 (2015).
- [25] S. Tamura, *J. Phys. Soc. Jpn.* **61**, 752 (1992).
- [26] P. Joy and S. Date, *J. Magn. Magn. Mater.* **210**, 31 (2000).
- [27] S. Singh, P. Pramanik, S. Sangaraju, A. Mallick, L. Giebeler, and S. Thota, *J. Appl. Phys.* **121**, 194303 (2017).
- [28] D. Wickham and W. Croft, *J. Phys. Chem. Solids* **7**, 351 (1958).
- [29] G. Blasse, *Philips Res. Rep.* **18**, 383 (1963).
- [30] N. Rajeevan, R. Kumar, D. Shukla, P. Thakur, N. Brookes, K. Chae, W. Choi, S. Gautam, S. Arora, I. Shvets *et al.*, *J. Phys.: Condens. Matter* **21**, 406006 (2009).
- [31] T.-C. Han, S.-S. Pan, and Y.-H. Liu, *J. Appl. Phys.* **116**, 244104 (2014).
- [32] P. Pramanik, S. Thota, S. Singh, D. C. Joshi, B. Weise, A. Waske, and M. Seehra, *J. Phys.: Condens. Matter* **29**, 425803 (2017).
- [33] P. Pramanik, D. Joshi, N. Tiwari, T. Sarkar, S. Pittala, O. Salman, M.-M. Manga, and S. Thota, *J. Appl. Phys.* **125**, 124302 (2019).
- [34] G. Bazuev and A. Korolyov, *J. Magn. Magn. Mater.* **320**, 2262 (2008).
- [35] D. Mandrus, V. Keppens, B. Chakoumakos, G. E. Granroth, and S. E. Nagler, *MRS Online Proc. Library* **547**, 177 (1998).
- [36] G. Granroth, D. Mandrus, V. Keppens, and S. Nagler, *J. Magn. Magn. Mater.* **272-276**, 1306 (2004).
- [37] S. Kaushik, N. Rajeevan, and R. Kumar, *Phys. B (Amsterdam)* **551**, 46 (2018).
- [38] J.-U. Hoffmann and M. Reehuis, *JLSRF* **4**, A129 (2018).
- [39] D. Töbrens, N. Stüßer, K. Knorr, H. Mayer, and G. Lampert, in *Materials Science Forum* Vol. 378 (Trans Tech, Zurich, 2001), pp. 288–293.
- [40] J. Rodriguez-Carvajal, *Phys. B (Amsterdam)* **192**, 55 (1993).
- [41] V. F. Sears, in *International Tables for Crystallography*, edited by A. J. C. Wilson (Kluwer Academic, Dordrecht, 1995), p. 383.
- [42] P. J. Brown, in *International Tables for Crystallography*, edited by A. J. C. Wilson (Kluwer Academic, Dordrecht, Dordrecht/Boston/London, 1995), p. 391.
- [43] S. Thota, M. Reehuis, A. Maljuk, A. Hoser, J.-U. Hoffmann, B. Weise, A. Waske, M. Krautz, D. Joshi, S. Nayak *et al.*, *Phys. Rev. B* **96**, 144104 (2017).
- [44] P. Pramanik, D. C. Joshi, M. Reehuis, A. Hoser, J. Hoffmann, R. Manna, T. Sarkar, and S. Thota, *J. Phys.: Condens. Matter* **32**, 245801 (2020).
- [45] W. Roth, *J. Phys. Chem. Solids* **25**, 1 (1964).
- [46] W. Jauch, M. Reehuis, H. J. Bleif, F. Kubanek, and P. Pattison, *Phys. Rev. B* **64**, 052102 (2001).
- [47] R. D. Shannon, *Acta Crystallogr., Sect. A* **32**, 751 (1976).
- [48] M. Reehuis, M. Tovar, D. M. Töbrens, P. Pattison, A. Hoser, and B. Lake, *Phys. Rev. B* **91**, 024407 (2015).
- [49] D. Jarosch, *Mineral. Petrol.* **37**, 15 (1987).
- [50] W. Roth, *J. Phys. (France)* **25**, 507 (1964).
- [51] B. Boucher, R. Buhl, R. Di Bella, and M. Perrin, *J. Phys. (France)* **31**, 113 (1970).
- [52] S. Guillemet-Fritsch, C. Tenaillieu, H. Bordeneuve, and A. Rousset, *Advances in Science and Technology* Vol. 67 (Trans Tech, Zurich, 2010), pp. 143–148.
- [53] B. Boucher, R. Buhl, and M. Perrin, *J. Appl. Phys.* **42**, 1615 (1971).
- [54] R. Chakravarthy, L. M. Rao, S. Paranjpe, S. Kulshreshtha, and S. B. Roy, *Phys. Rev. B* **43**, 6031 (1991).
- [55] N. S. S. Murthy, M. G. Natera, S. I. Youssef, R. J. Begum, and C. M. Srivastava, *Phys. Rev.* **181**, 969 (1969).
- [56] K. H. Jani, K. Modi, H. Joshi, P. Babu, and S. Paranjpe, *J. Magn. Magn. Mater.* **280**, 334 (2004).
- [57] S. Yunus, H.-S. Shim, C.-H. Lee, M. Asgar, F. Ahmed, and A. Zakaria, *J. Magn. Magn. Mater.* **241**, 40 (2002).
- [58] V. O. Garlea, R. Jin, D. Mandrus, B. Roessli, Q. Huang, M. Miller, A. J. Schultz, and S. E. Nagler, *Phys. Rev. Lett.* **100**, 066404 (2008).
- [59] K. Matsuura, H. Sagayama, A. Uehara, Y. Nii, R. Kajimoto, K. Kamazawa, K. Ikeuchi, S. Ji, N. Abe, and T.-h. Arima, *Phys. Rev. Lett.* **119**, 017201 (2017).
- [60] E. Winkler, S. Blanco Canosa, F. Rivadulla, M. A. López-Quintela, J. Rivas, A. Caneiro, M. T. Causa, and M. Tovar, *Phys. Rev. B* **80**, 104418 (2009).
- [61] P. Aleshkevych, M. Baran, S. Barilo, J. Fink-Finowicki, and H. Szymczak, *J. Phys.: Condens. Matter* **16**, L179 (2004).
- [62] L. Yan, W. Ren, J. Shen, Z. Sun, and F. Wang, *J. Appl. Phys.* **105**, 07A719 (2009).